

The Cluster AgeS Experiment (CASE).[†] Detecting Photometric Variability with the Friends of Friends Algorithm^{*}

M. R o z y c z k a¹, W. N a r l o c h¹,
P. P i e t r u k o w i c z² I. B. T h o m p s o n³ and
W. P y c h¹

¹Nicolaus Copernicus Astronomical CENter of the Polish Academy of
Sciences, ul. Bartycka 18, 00–716 Warsaw, Poland
e-mail: (mnr, pych, wnarloch)@camk.edu.pl

²Warsaw University Observatory, Al. Ujazdowskie 4, 00-478 Warsaw, Poland
e-mail: pietruk@astrouw.edu.pl

³The Observatories of the Carnegie Institution for Science, 813 Santa Barbara
Street, Pasadena, CA 91101, USA
e-mail: ian@obs.carnegiescience.edu

ABSTRACT

We adapt the friends of friends algorithm to the analysis of light curves, and show that it can be successfully applied to searches for transient phenomena in large photometric databases. As a test case we search OGLE-III light curves for known dwarf novae. A single combination of control parameters allows to narrow the search to 1% of the data while reaching a ~90% detection efficiency. A search involving ~2% of the data and three combinations of control parameters can be significantly more effective - in our case a 100% efficiency is reached.

The method can also quite efficiently detect semi-regular or strictly periodic variability. We report 28 new variables found in the field of the globular cluster M22, which was examined earlier with the help of periodicity-searching algorithms.

Methods: data analysis – Stars: variables – globular clusters: individual (M22) – Galaxy: disk binaries: close novae, cataclysmic variables

1 Introduction

The friends-of-friends method (FoF) was introduced in cosmology by Turner & Gott (1976) as a tool to identify clusters of galaxies. In FoF, a cluster is defined using the clustering length CL such that each member galaxy has at least one neighbor at a distance $d \leq CL$. In other words, for each galaxy all neighbors closer than the CL -threshold are members of the cluster which that galaxy belongs to.

The basic algorithm of the method was published by Huchra & Geller (1982). Although several more sophisticated approaches to the clustering problem have been developed, FoF is still widely used for its simplicity and effectiveness. Its another advantage is that it uniquely assigns galaxies to clusters, while making no assumptions on cluster properties. Obviously, for a given sample of galaxies both the number and the richness of FoF clusters depend on CL , so that a calibration is necessary. In fact, beginning with Huchra & Geller (1982), two clustering lengths have been used in most implementations: $CL_{\perp} = b_{\perp} * s(z)$ for

[†]CASE was initiated and for long time led by our friend and tutor Janusz Kaluzny, who prematurely passed away in March 2015.

^{*}Based on data obtained with Swope and Warsaw telescopes at Las Campanas Observatory.

distances in the plane of the sky, and $CL_{\parallel} = b_{\parallel} * s(z)$ for distances along the line of sight, where $s(z)$ is the redshift-dependent mean three-dimensional separation between galaxies, and $(b_{\perp}, b_{\parallel})$ are scaling parameters to be calibrated. Surveys performed since 2010 and reviewed by Duarte & Mamon (2014) yielded b_{\perp} and b_{\parallel} ranging from 0.06 to 0.11 and from 0.67 to 1.1, respectively, with b_{\parallel} consistently larger than b_{\perp} to account for redshift space distortions (the so-called Fingers of God). In the same paper Duarte & Mamon derived $b_{\perp} \simeq 0.11$ and $b_{\parallel} \approx 1.3$ using a mock galaxy catalog generated from cosmological simulations.

The aim of the present contribution is to show that FoF can be successfully applied to the search for aperiodic variations in long series of photometric measurements. In the epoch of massive photometry and robotic telescopes many algorithms capable of detecting this type of variability, with particular emphasis on sudden brightenings, have been developed. A related review has recently been published by Sokolovsky et al. (2017), and there is no need to repeat their extensive discussion. We only mention that they test 18 statistical characteristics of brightness measurements, and compare their performance in identifying variable objects on several data sets with time-series photometry. FoF-based search for variability can be a useful additional technique.

The implementation of the algorithm is outlined in Section 2. Control parameters of FoF are calibrated in Section 3, and in Section 4 the method is applied to light curves collected within CASE in the field of the globular cluster M22. In Section 5 we estimate the detection efficiency of FoF based on OGLE-III light curves surveyed by Mróz et al. (2013, hereafter MP13), and Pietrukowicz et al. (2013). A brief summary of the paper is presented in Section 6.

2 Implementation of the algorithm

Our original idea was to write a code capable of identifying irregularly “flashing” objects, e.g. dwarf novae (DN), and the mathematical problem we posed was the following: given a set \mathcal{S} of time-sorted measurements $V_i(t_i)$

- divide it into clusters G_k of points $p_i = (t_i, V_i)$ such that

$$p_i \in G_k \wedge d_{ij} \leq CL \Rightarrow p_j \in G_k,$$

where d_{ij} is the distance between p_i and p_j , and CL is the assumed clustering length,

- and identify the brightest, or “peak” cluster G_p which most strongly deviates from the median $\text{Md}(V)$ of all measurements in \mathcal{S} .

To find the solution, a reasonable definition of distances is necessary. Our approach involves the following steps:

1. Compress the time axis by removing all Julian days without measurements. Define the normalized time $\tau_i = (t_i - t_1)/(t_L - t_1)$, where t_L and t_1 are Julian dates of the last and first measurement, respectively. Remove points with $V > \text{Md}(V)$ (this optional operation saves the CPU time, and biases the variability search towards brightenings which we are mainly interested in). Define the normalized magnitude $v_i = (\text{Md}(V) - V_i)/(\text{Md}(V) - V_{min})$, where V_{min} is the magnitude of the brightest point in \mathcal{S} (note that v increases with increasing brightness). All the points are now located within a unit square (see Fig. 1), and the distance d_{ij} can be defined as the Cartesian distance between (τ_i, v_i) and (τ_j, v_j) .

2. Compute all distances d_{ij} . Find the mean distance \bar{d} , and the clustering length $CL = b\bar{d}$, where b is a control parameter corresponding to b_{\perp} from Sect. 1. Draw a virtual circle of radius CL around each p_i . Merge each set of overlapping circles into a cluster.
3. Reject clusters comprising fewer than N_M points, where N_M is another control parameter. For each remaining cluster G_k find the minimum v_k^{min} , and the mean \bar{v}_k . Identify the peak cluster G_p as the one for which $v_p^{min} = \max_k(v_k^{min})$.

Based on v_p^{min} and the corresponding \bar{v}_p , the variability index ν can be calculated, which we define as

$$\nu = \begin{cases} v_p^{min} & \text{if } v_p^{min} < 0.4 \\ \bar{v}_p & \text{otherwise.} \end{cases}$$

Adopting such a definition, we have $1.0 \geq \nu \geq 0.0$, where larger values indicate the presence of at least one brightening episode, and smaller values suggest that the examined star does not vary in brightness. The cutoff at $v_p^{min} = 0.4$ is introduced based on calibration results from the next Section, and its aim is to avoid assigning $\nu > 0$ to stars with $v_p^{min} = 0$.

Note that the smaller b is, the more densely populated areas of the (τ, v) plane are only sampled, and, for a nonvariable source, the smaller is the chance to generate spurious clusters with $v_k^{min} > 0$ which would artificially increase the variability index. Obviously, if b is too small for a given N_M then no clusters will be found. On the other hand, when b is too large, real clusters with $v_k^{min} > 0$ may be spuriously extended to include points with $v \approx 0$, causing the physical variability to be classified as a noise. In any case, the control parameters b and N_M should be so chosen that G_p contains sufficiently many points to represent a real physical increase in brightness.

3 Calibrating FoF

For the calibration, observations of the globular cluster M22 collected within the CASE project (Kaluzny et al. 2005), and searched for periodic variability by Rozyczka et al. (2017; hereafter R17) were used. R17 examined light curves of almost 124,000 stars with $V \lesssim 22$ mag, identifying over 350 periodic or likely periodic variables, and a few likely long-term variables. 238 of these were new detections.¹

Trial runs performed on various subsets of this data with several values of clustering parameter b and minimum size of the cluster N_M yielded four new variables, which together with a BL Her - type pulsator described by R17 (hereafter star #24), and a randomly picked constant member of M22 (hereafter star C1), provided input to the calibration procedure. The aim of the calibration was to find optimal values of b and N_M , at which the physical variability is most easily detectable. The results are shown in Fig. 2, where ν is plotted for all the six stars as a function of b for $N_M = 5, 10$ and 15 .

Stars U70 and N188 (red and green lines), which have evidently ‘‘peaking’’ light curves (see Fig. 3), nicely illustrate the dependence of ν on b discussed in Sect. 2. As the clustering length increases, more and more points are added

¹Data for all the identified variables are available at <http://case.camk.edu.pl>

to the peak cluster causing v_p^{min} , \bar{v}_p , and consequently ν , to decrease. At $b=0.17$ the peak cluster of U70 merges with the rest of the light curve, and the brightening of the star for $HJD > 2451770$ becomes undetectable, while the brightening of N188 can be detected until $b=0.3$ (but most probably not much farther).

N184 is a semiregular B-type OSARG (Wray et al. 2004) whose variability was not detected by AOV algorithms of R17, while star #24 exhibits strictly periodic oscillations (which are not evident in Figs. 3 and 4 because their period of 1.715 d is too short). In both cases (blue and cyan lines in Fig. 2) $\nu > 0.75$ is observed for $0.1 < b < 0.29$ independently of N_M . This somewhat surprising bonus of the method shows that FoF can also quite efficiently detect various cases of a more regular variability. The necessary condition for it to perform well on semiregular or periodic light curves is that at least one maximum must be well sampled.

An even more surprising detection of variability occurred in the case of V136 (magenta line in Fig. 2). At a first glance, the light curve looks immune to FoF: Figs. 3 and 4 show a roughly sinusoidal brightness change with an amplitude barely larger than the observational noise, of which a half of the period is only covered. However, the densely populated core of the broad maximum of the curve is located above the median $Md(V)$. Since a small b probes the densest regions of the (τ, v) plane, for all N_{min} the corresponding peak cluster resides in the core, yielding $\nu > 0$. With a larger b another, more loosely bound peak cluster is found, located higher up in the less densely populated envelope of the maximum, causing an increase in ν . For $b > 0.135$ the peak cluster merges with the rest of the light curve, and the subtle variability of V136 ceases to be detectable for FoF. The secondary maximum at $0.15 < b < 0.22$ and plateau at $b > 0.22$ originate from small groups of points with largest observational errors at $HJD 2451692$ and $HJD 2451773$, respectively. A similar spurious variability is observed for the constant star C1 (black line). However, while for $N_M = 5$ it is detectable in the whole range of b , for increasing N_M the effect is limited to a narrower and narrower subrange.

We conclude that the optimum value of b lies between 0.02 and 0.04, i.e. in a range in which the clearly physically variable stars U70, N188, N184, and #24 have the largest variability index. Encouragingly, for $5 \leq N_M \leq 15$ the results of variability search depend rather weakly on the minimum size of the cluster. Some precaution is advisable, however. As Fig. 2 indicates, adopting smaller values from this range may increase the probability of false detections, while at larger values the variability index of real physical variables may be slightly underestimated. One must also remember that even $\nu = 1$ does not guarantee that the star is physically variable. All FoF can do is to select from a large sample of stars a smaller subsample of candidate variables whose light curves must be visually inspected. The question of how large this subsample should be, i.e. down to which ν the inspection should continue, will be answered in the next chapter.

4 Search for new variables in the M22 field

Encouraged by the results of the trial runs, we decided to conduct a thorough search for new variables in M22. All the known variables were removed from the light curve collection of R17, and for the remaining stars the variability index ν was calculated using $N_M = 5$, and $b = 0.03$. The stars were sorted according to

the decreasing ν , and the first 3700 light curves (i.e. three per cent of the total) were visually inspected.

Twenty eight new variables and two suspected variables were found, whose basic parameters are given in Table 1. For the naming convention to agree with that of R17, they are given designations V136 (a likely member of M22), U70 (a star whose membership status is unknown), and from N176 on (field stars). The membership criteria are the same as in R17 - mainly based on proper motion measurements presented in Narloch et al. (2017; hereafter N17). Stars #24 and C1 are included in Table 1 as the objects used for code calibration in Sect. 3. The equatorial coordinates in columns 2 and 3 conform to the UCAC4 system (Zacharias et al. 2013), and are accurate to $0''.2 - 0''.3$. Columns 4–7 contain average V -band magnitude \bar{V} , $\bar{B} - \bar{V}$ color, full amplitude in the V -band, and membership status. In the next two columns variability type and variability index ν are given. The last column gives detectability coefficients $\delta = N_s/N_{lc} * 100$, where N_s is the sequential number of a star on a list of stars sorted according to the decreasing ν , and $N_{lc}=123,775$ is the total number of the examined lightcurves (note that smaller values of δ indicate better detectability).

A CMD of M22 with locations of the new variables is shown in Fig. 5. The gray background stars are PM-members of M22 identified by N17. The only new likely member of the cluster is the red giant V136 described in Sect. 3. The most interesting object in the sample is undoubtedly U70, which between HJD 2451765 and HJD 2451783 brightened by ~ 2.3 mag, and remained in this state for at least 15 d. Compelling explanations for such a behavior are DN eruption or microlensing effect. If U70 was a member of M22, then for $(m - M)_V = 13.6$ mag and $E(B - V) = 0.34$ mag (Harris 1996, 2010 edition) its extinction-corrected absolute magnitude at maximum would be $M_V \sim -5.5$ mag - a lowish, but still acceptable value for a DN (Patterson 2011). On the other hand, no X-ray source is located within $30''$ from U70 (Rosen et al. 2016), and no indication for a color change between low and high state of U70 is observed, which rather speaks for the gravitational lens hypothesis. Unfortunately, because of the large scatter of measurements and incomplete coverage of the light curve we are not able to distinguish between these two possibilities. In any case, this is the fourth transient in the M22 field, the first three having been detected by Pietrukowicz et al. (2005).

Proper motions indicate that all the remaining stars from Table 1 except C1 and #24 are field objects (N17). Most of them are OSARGs of type B, evident exceptions being type A OSARGs N189 and N201. The light curve of N184 in Figs. 3 and 4 is typical of OSARG-B objects. An example OSARG-A light curve is shown in Fig. 6 along with another two curves of stars from Table 1, and the B -band light curve of U70.²

Twenty-nine variables have $\delta < 1.0$, i.e. they belong to the first percentile of the whole set of light curves sorted according to the decreasing ν . In the second percentile there is only one star - the suspected variable N182. Similarly, V136 is the only star in the third percentile. Based on these results one may expect that using FoF can reduce the number of stars that have to be individually inspected to about one hundredth of a given data set. An obvious practical rule is to stop inspecting when the function $N_{var}(N_s)$ flattens, where N_{var} is the number of detected physical variables, and N_s is the sequential number of a star in the sorted data set.

²Light curves of all the variables from Table 1 are available at <http://case.camk.edu.pl>

5 Performance of FoF on OGLE-III light curves

To independently assess the potential of FoF, and estimate the efficiency with which it can detect eruptive variables, we applied it to the set of over 345,000 light curves from twenty one OGLE-III Galactic disk fields (Szymanski et al. 2010), in which 40 new dwarf novae were identified by MP13.

The whole set was divided into seven subsets differing considerably in time coverage and number of observations, and, to a lesser extent, in density of stellar images and/or photometric quality (see Pietrukowicz et al. 2013). For all stars in each subset the variability index was computed using $(N_M, b) = (5, 0.03)$. Next, each subset was sorted according to the decreasing ν , sequential numbers n_{DN} of OGLE-III DNe in the so-obtained sequence were found, and detectability coefficients $\delta = n_{\text{DN}}/N_{\text{Ic}} * 100$ were calculated, where N_{Ic} is the number of light curves in the subset. The results are given in the 4th column of Table 2. In five cases δ is larger than 1, meaning that 35 DNe (87.5% of the total) would be found if the search was limited to $\delta_{\text{max}} = 1\%$, i.e. to the first percentile of the whole data set. All DNe would be found only with $\delta_{\text{max}} \approx 16\%$, implying less than a tenfold reduction in the number of the light curves to be inspected.

To see how these results depend on control parameters, we made additional runs using $(N_M, b) = (5, 0.02)$ and $(10, 0.02)$. Respective detectability coefficients are listed in columns 5 and 6 of Table 2. In both cases three DNe remain undetected, i.e. the overall detection efficiency increases to 92.5%. Altogether, with $\delta_{\text{max}} = 1\%$ thirty one DNe are detected in all three (N_M, b) runs, and further seven DNe in two runs. The remaining two DNe, OGLE-GD-DN-011 and OGLE-GD-DN-038, are found in single runs only. Their light curves have a poorer than average quality, but they are not really the poorest ones in the collection of MP13. Additional factor(s) must influence their detectability, e.g. the number of objects (including artefacts) with ν larger than that of either of the two DNe.

The DN light curves of MP13 significantly differ from each other in time-coverage, average sampling density, and photometric accuracy, and display a rich variety of shapes. As such, they may be regarded as a fairly representative sample, allowing for the generalization of our findings. Thus, we expect that in surveys comparable in quality to OGLE about ten per cent of DNe (and, probably, of eruptive variables in general) may remain undetected by FoF if only one combination of control parameters (N_M, b) is used with $\delta_{\text{max}} = 1\%$, i.e. if one does not intend to inspect more than 1% of the light curves. While a detection efficiency of $\sim 90\%$ seems quite acceptable, at least in some cases it can be increased to nearly 100% when a *combined search* involving output from runs with different control parameters is applied (note that in our survey each DN is detected in at least one run with $\delta_{\text{max}} = 1\%$). The corresponding Unix procedure consists of the following three steps:

1. Sort the output from each run over decreasing ν , and select the first 1% of stars. Write *id* and ν of each selected star to file A. Sort A over decreasing ν . *Optionally, remove stars with $\nu \approx 0$ from A.* Write *ids* of stars from file A to file B.
2. Apply the command `sort -u B -o B` which removes repeated *ids* from B (in our survey, B gets shorter by up to 40%). In the Bash Shell apply the command `for a in `cat B`; do grep -ml $a A; done > C`, which for each star from B finds the first occurrence of its *id* in A, and writes the corresponding record to C.

3. Sort C over decreasing ν , and overwrite B with star *ids* from C. Inspect light curves of stars from B.

With such an arrangement, stars found by FoF to be most likely variable will be inspected first. The results of our combined search for DNe are displayed in Table 3 which for each data subset identified in column 1 gives the number of stars in file B (column 2), percentage of stars from file B in the data subset (column 3), and percentage of stars from file B that would have to be inspected before *all* OGLE-III DNe from the given subset were found (column 4). As the last row of Table 3 shows, all DNe can be identified at the expense of going through about 2% of the light curves. One should remember, of course, that the combined search does not warrant a 100% success in all cases. One can be sure, however, that in general its detection efficiency will be higher than that of a search based on a single combination of FoF control parameters.

6 Summary

We have shown that the FoF algorithm adapted to the analysis of light curves can be successfully applied to searches for transient or aperiodic phenomena in large photometric databases. Given the control parameters N_M and b introduced in Section 2, our implementation of FoF assigns to each curve the variability parameter ν with a value between 0 and 1, with larger values indicating the presence of at least one brightening episode, and smaller values suggesting that the examined star does not vary in brightness. A test conducted on dwarf novae found by MP13 in OGLE-III data allows to estimate the detection efficiency of our implementation at $\sim 90\%$ when the search is limited to the first 1% of light curves sorted over decreasing ν , and only one combination of control parameters is used. A search involving $\sim 2\%$ of light curves and three combinations of control parameters can be significantly more effective - in our test case all OGLE-III dwarf novae were identified.

We believe FoF is a useful tool, but we are aware of its limitations. In particular, potential users must remember that it does not distinguish between observational artefacts and physical variability, and for this reason it may perform rather poorly on noisy data. Also, we cannot be sure that the values of N_M and b parameters used in the present paper would be the best choice for all light curve collections. We rather suggest to perform a calibration like that in Section 3 every time a new data set is analyzed.

Finally, we mention that upon calibrating the control parameters we realized that FoF can also quite efficiently detect semi-regular or strictly periodic variability. In Section 4 we report 28 new variables found in the field of the globular cluster M22, which had been examined earlier by R17 using periodicity-searching algorithms. New transient, semi-regular or periodic variables found in the OGLE-III data will be reported elsewhere.

Acknowledgements. PP was supported from the Polish National Science Centre grant MAESTRO 2014/14/A/ST9/00121. We thank Joe Smak for useful comments, and Grzegorz Pojmański for the lc code which vastly facilitated the work with light curves.

REFERENCES

- Harris, W.E. 1996, *Astron. J.*, **112**, 1487.
- Huchra, J. P., and Geller, M. J. 1982, *Astrophys. J.*, **257**, 423.
- Kaluzny, J., Thompson, I. B., Krzeminski, W., Preston, G. W., Pych, W. et al. 2005, *Stellar Astrophysics with the Worlds Largest Telescopes, AIP Conf. Proc.*, **752**, 70.
- Mróz, P., Pietrukowicz, P., Poleski, R., Udalski, A., Soszyński, I. et al. 2013, *Acta Astron.*, **63**, 135 (MP13).
- Narloch, W., Kaluzny, J., Poleski, R., Rozyczka, M., Pych, W., and Thompson, I. B. 2017, *MNRAS*, **471**, 1476 (N17).
- Patterson, J. 2011, *MNRAS*, **411**, 2695.
- Pietrukowicz, P., Kaluzny, J., Thompson, I. B., Jaroszynski, M., Schwarzenberg-Czerny, A. et al. 2005, *Acta Astron.*, **55**, 261.
- Pietrukowicz, P., Mróz, P., Soszyński, I., Udalski, A., Poleski, R. et al. 2013, *Acta Astron.*, **63**, 115.
- Rosen, S. R., Webb, N. A., Watson, M. G., Ballet, J., Barret, D. et al. 2016, *Astron. Astrophys.*, **590**, A1.
- Rozyczka, M., Thompson, I. B., Pych, W., Narloch, W., Poleski, R. and Schwarzenberg-Czerny, A. 2017, *Acta Astron.*, **67**, 203 (R17).
- Sokolovsky, K. V., Gavras, P., Karamelas, A., Antipin, S. V., Bellas-Velidis, I. et al. 2017, *MNRAS*, **464**, 274.
- Szymański, M. K.; Udalski, A.; Soszyński, I.; Kubiak, M.; Pietrzyński, G. et al. 2010, *Acta Astron.*, **60**, 295.
- Turner, E. L., and Gott, J. R. 1976, *Astrophys. J. Suppl. Ser.*, **32**, 409.
- Wray, J. J., Eyer, L., and Paczyński, B. 2004, *MNRAS*, **349**, 1059.
- Zacharias, N., Finch, C. T., Girard, T. M., Henden, A., Bartlett, J. L. et al. 2013, *Astron. J.*, **145**, 44.

Table 1: Basic data of FoF variables discovered in the field of M22

ID	RA [deg]	DEC [deg]	V [mag]	$B - V$ [mag]	Δ_V [mag]	Mem ^a	Type ^b	ν^c	δ^d [%]
V136	279.16521	-23.87854	13.93	1.07	0.02	Y	V	0.34	2.50
U70 ^e	278.98646	-23.90984	22.46	0.50	2.30	U	V	0.89	0.04
U70	278.98646	-23.90984	20.16	0.47	2.30	U	V	0.89	0.04
N176	279.19779	-23.73977	15.05	1.84	0.28	N	V	0.93	0.03
N177	279.21259	-23.83521	14.11	1.75	0.07	N	V	0.93	0.03
N178	279.20565	-23.91109	14.11	1.76	0.13	N	V	0.88	0.04
N179	279.19954	-23.89914	13.42	1.81	0.02	N	S	0.42	0.90
N180	279.22549	-23.93757	16.66	1.87	0.42	N	V	0.93	0.03
N181	279.20120	-24.05648	13.61	1.81	0.09	N	V	0.87	0.04
N182	279.12222	-23.80253	14.69	1.65	0.03	N	S	0.37	1.53
N183	279.13698	-23.88486	16.72	1.16	0.16	N	V	0.63	0.11
N184	279.15103	-23.92146	14.76	1.81	0.39	N	V	0.98	0.01
N185	279.14376	-23.96482	15.02	1.73	0.58	N	V	0.96	0.01
N186	279.15241	-24.01048	13.92	1.73	0.12	N	V	0.86	0.04
N187	279.11106	-23.75086	15.06	1.42	0.23	N	V	0.79	0.06
N188	279.04501	-23.76959	14.44	1.82	0.06	N	V	0.97	0.01
N189	279.09219	-23.81836	14.65	1.79	0.03	N	V	0.69	0.09
N190	279.07769	-23.83870	15.35	1.71	0.21	N	V	0.95	0.02
N191	279.07322	-23.83017	16.11	1.76	0.56	N	V	0.95	0.02
N192	279.05198	-23.92851	15.41	1.58	0.25	N	V	0.88	0.04
N193	279.08704	-23.97307	14.50	1.74	0.04	N	V	0.61	0.14
N194	279.07205	-23.98484	13.67	1.70	0.15	N	V	0.93	0.03
N195	279.07035	-24.09773	15.31	1.73	0.42	N	V	0.95	0.02
N196	278.98961	-23.73304	16.00	1.78	0.61	N	V	0.97	0.01
N197	279.00753	-23.79984	17.07	1.75	0.23	N	V	0.89	0.03
N198	278.97410	-23.84254	13.92	1.75	0.31	N	V	0.94	0.02
N199	279.01856	-23.86728	15.57	1.77	0.07	N	V	0.94	0.02
N200	279.01240	-23.87550	15.80	1.80	0.37	N	V	0.90	0.03
N201	279.01744	-23.98125	13.84	1.71	0.04	N	V	0.92	0.03
N202	278.99578	-23.99937	14.41	1.20	0.04	N	V	0.80	0.06
N203	278.97643	-24.05441	15.98	1.62	0.29	N	V	0.70	0.08
#24	279.09078	-23.90371	13.42	0.90	0.65	Y	V	0.93	0.03
C1	279.08297	-23.86369	18.94	0.70	0.30	Y	C	0.13	77.4

^a Membership status: Y - member, U - no data or data ambiguous, N - field object.

^b V - variable, S - suspected variable, C - constant star.

^c Variability index defined in Sect. 2, obtained for $N_M=5$ and $b=0.03$.

^d δ is the percentage of lightcurves sorted over decreasing ν that has to be inspected before the star indicated in the first column is encountered.

^e For U70, magnitude and color at low and high state are given.

Table 2: Detectability of OGLE-III galactic disk dwarf novae

Object	Data subset ^a	N_{lc}	(N_M, b)		
			(5, 0.03) δ^b [%]	(5, 0.02) δ [%]	(10, 0.02) δ [%]
OGLE-GD-DN-001	CAR115-118	25048	0.03	0.03	0.01
OGLE-GD-DN-002	CAR115-118	25048	0.55	0.22	0.06
OGLE-GD-DN-003	CAR115-118	25048	0.01	0.00	0.02
OGLE-GD-DN-004	CAR115-118	25048	0.05	0.04	0.04
OGLE-GD-DN-005	CAR115-118	25048	0.38	0.14	0.04
OGLE-GD-DN-006	CAR115-118	25048	1.01	0.62	0.17
OGLE-GD-DN-007	CAR115-118	25048	0.45	0.20	0.06
OGLE-GD-DN-008	CAR115-118	25048	0.28	0.02	0.10
OGLE-GD-DN-009	CAR107-110	34475	0.12	0.03	0.01
OGLE-GD-DN-010	CAR107-110	34475	0.01	0.01	0.03
OGLE-GD-DN-011	CAR107-110	34475	0.20	2.58	10.09
OGLE-GD-DN-012	CAR107-110	34475	0.22	0.07	0.06
OGLE-GD-DN-013	CAR111-114	88975	0.15	0.08	0.04
OGLE-GD-DN-014	CAR111-114	88975	0.15	0.02	0.00
OGLE-GD-DN-015	CAR107-110	34475	0.06	0.03	24.17
OGLE-GD-DN-016	CAR107-110	34475	0.35	0.20	0.05
OGLE-GD-DN-017	CAR100-105	78558	0.30	0.18	0.05
OGLE-GD-DN-018	CAR100-105	78558	0.94	0.40	0.11
OGLE-GD-DN-019	CAR100-105	78558	0.09	0.22	0.07
OGLE-GD-DN-020	CAR100-105	78558	1.28	0.07	0.19
OGLE-GD-DN-021	CAR100-105	78558	0.90	0.40	0.21
OGLE-GD-DN-022	CAR100-105	78558	0.23	0.08	0.02
OGLE-GD-DN-023	CAR100-105	78558	3.40	0.55	0.14
OGLE-GD-DN-024	CAR111-114	88975	0.25	0.13	0.05
OGLE-GD-DN-025	CAR111-114	88975	0.12	0.12	0.04
OGLE-GD-DN-026	CAR111-114	88975	0.53	0.29	0.08
OGLE-GD-DN-027	CAR111-114	88975	0.04	0.26	76.19
OGLE-GD-DN-028	CAR111-114	88975	0.04	0.02	0.06
OGLE-GD-DN-029	CAR106	8710	0.29	0.24	0.11
OGLE-GD-DN-030	CAR100-105	78558	0.01	0.00	0.01
OGLE-GD-DN-031	CAR100-105	78558	0.93	0.55	0.45
OGLE-GD-DN-032	CEN106-107	26271	0.01	0.01	0.00
OGLE-GD-DN-033	CEN108-MUS	83423	0.36	0.11	0.04
OGLE-GD-DN-034	CEN108-MUS	83423	0.58	0.04	0.11
OGLE-GD-DN-035	CEN108-MUS	83423	0.67	0.30	0.11
OGLE-GD-DN-036	CEN108-MUS	83423	1.12	0.49	0.36
OGLE-GD-DN-037	CEN108-MUS	83423	0.02	0.01	0.20
OGLE-GD-DN-038	CEN108-MUS	83423	15.62	1.01	0.32
OGLE-GD-DN-039	CEN108-MUS	83423	0.11	1.12	0.47
OGLE-GD-DN-040	CEN108-MUS	83423	0.11	0.02	0.03

^a Identified by OGLE-III disk fields from which the light curves of MP13 were extracted.

^b δ is the percentage of the sorted data subset indicated in the second column that has to be inspected before the dwarf nova indicated in the first column is encountered. $\delta=0$ means that less than 0.01% of the data subset has to be inspected.

Table 3: Results of the combined search*

Data subset	N_B	N_B/N_{1c} [%]	N_{all}/N_B [%]
CAR100-105	1451	1.8	58.3
CAR106	163	1.9	15.3
CAR107-110	625	1.8	19.8
CAR111-114	1932	2.2	12.1
CAR115-118	488	1.9	58.2
CEN106-107	575	2.2	00.5
CEN108-MUS	1489	1.8	79.5
Total	6723	1.9	

* See text for explanations.

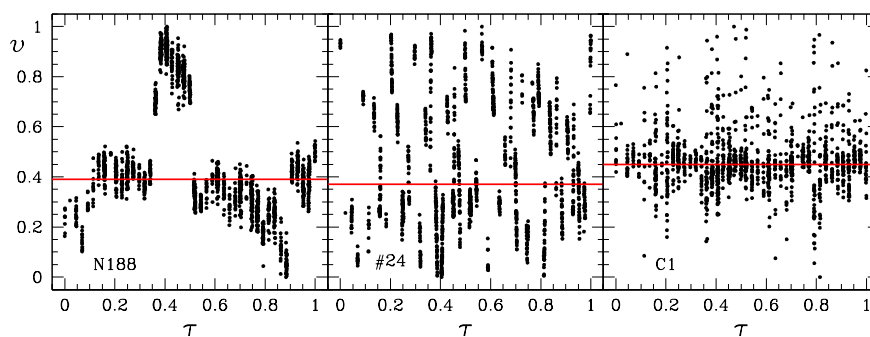


Figure 1: Examples of normalized light curves (see text for explanations). Red lines mark median values of v . Labels within the frames identify stars described in Section 3.

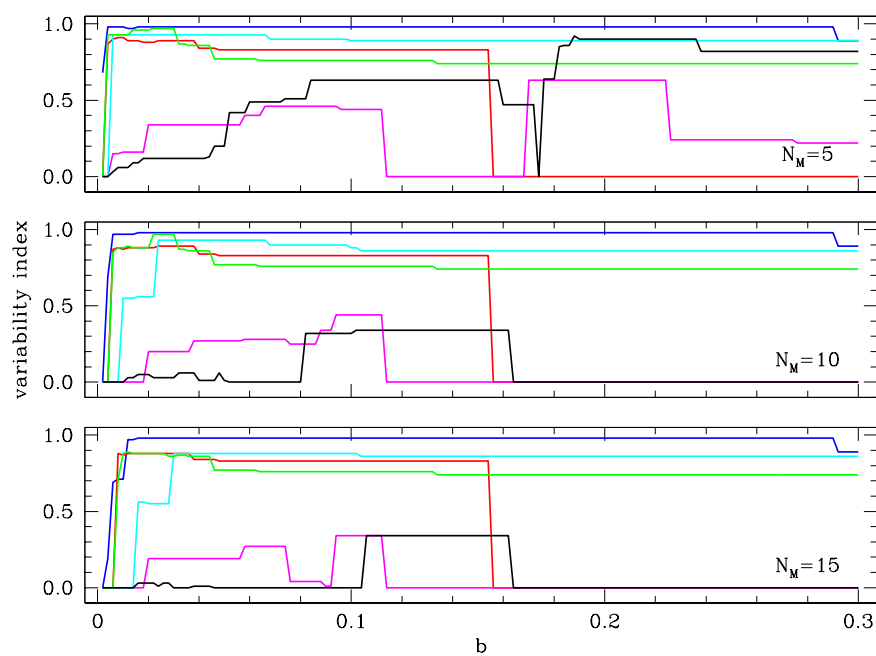


Figure 2: Variability index as a function of clustering length parameter b and minimum size of the cluster N_M for stars U70, N188, N184, #24, V136 and C1 from the M22 field (red, green, blue, cyan, magenta and black curves, respectively).

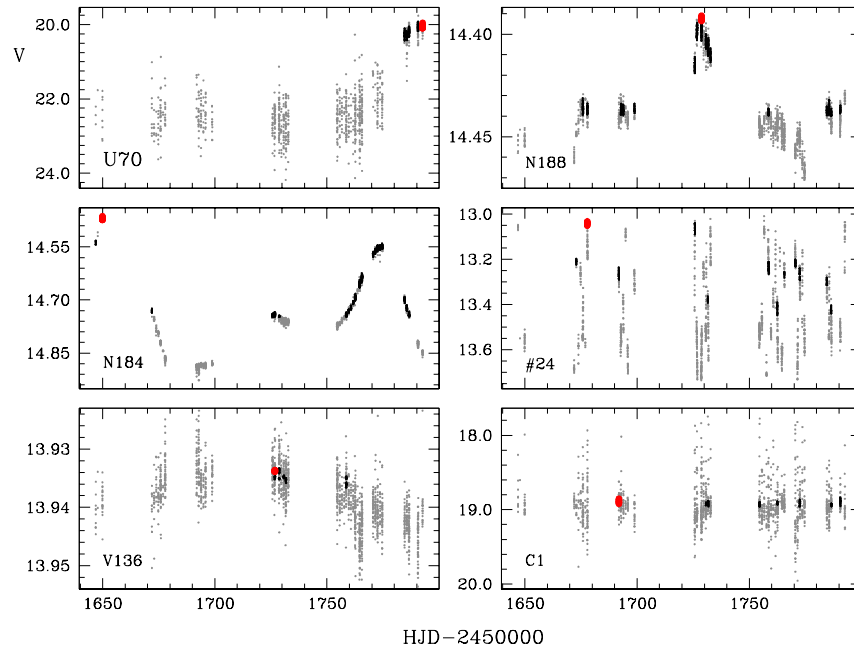


Figure 3: Top left to bottom right: raw curves of stars U70, N188, N184, #24, V136 and C1. Grey: points located below the median $M_d(V)$ or belonging to clusters with less than $N_M = 10$ members. Black or red: points belonging to clusters with at least N_M members. Red: the brightest cluster, based on which the variability index is defined. Results obtained for $b = 0.03$.

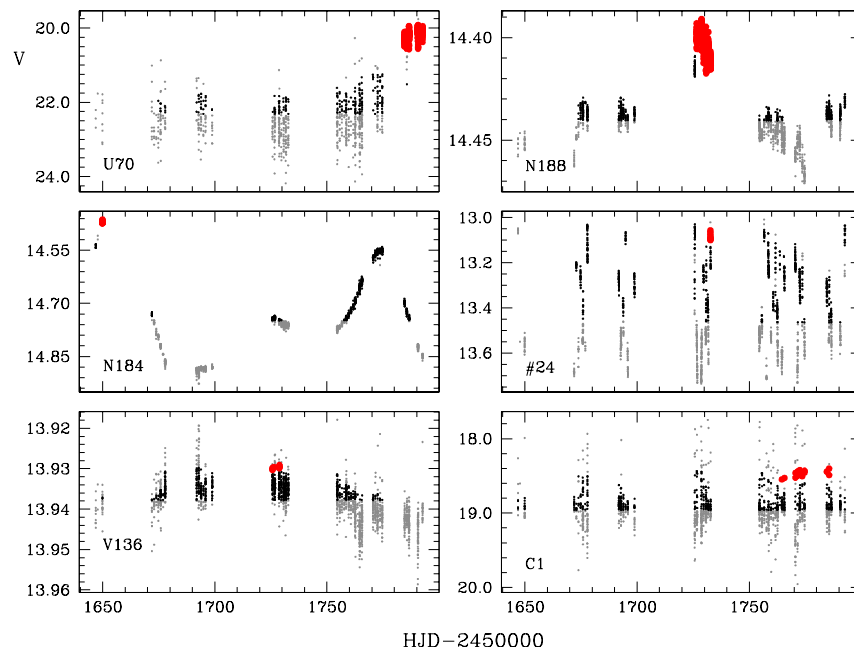


Figure 4: Same as Fig. 3 for $b = 0.1$

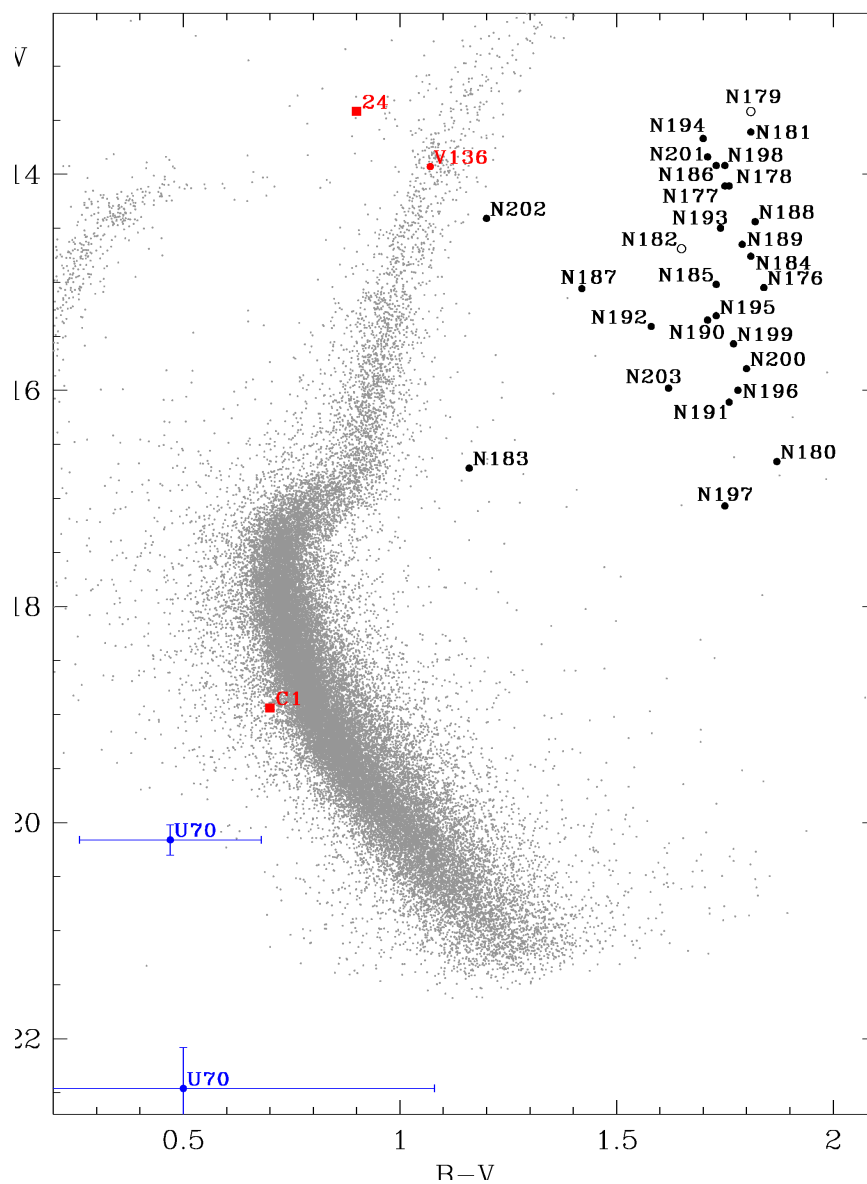


Figure 5: CMD for the M22 field with locations of FoF-detected variables. Red: Members or likely members of M22; blue: stars of unknown membership; black: field stars. Filled circles: confirmed variables; open circles: suspected variables. Squares: stars included in Figs. 2–4 for code-testing purposes. C1 is constant; star #24 is a BL Her - type variable described by R17. Star U70 is shown at minimum and maximum light. The gray background stars are PM-members of M22 identified by N17.

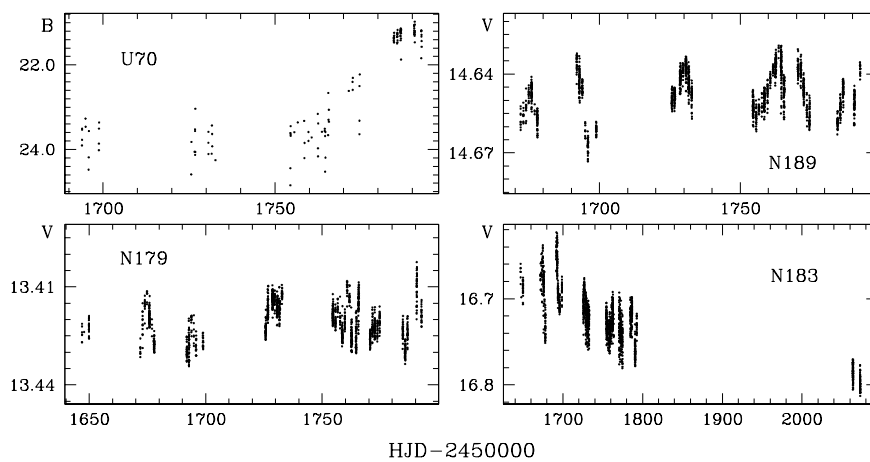


Figure 6: Top left to bottom right: *B*-band light curve of star U70, and *V*-band light curves of stars N189, N179 and N183 - examples of, respectively, OSARG-A, suspected variable, and long-term variable from Table 1.